Correlation Analysis of Waves above a Capacitive Plasma Applicator

W. Gekelman,[1] M. Barnes,[2] S. Vincena,[1] and P. Pribyl[1]

[1]*Department of Physics and Astronomy, University of California, Los Angeles, California, USA*
[2]*Intevac Corporation, Santa Clara, California, USA*
(Received 20 April 2009; published 22 July 2009)

Capacitively coupled plasma glow discharges have been extensively used for materials processing in numerous industrial applications. Considerable research has been performed on plasma sheaths and standing waves over a capacitive applicator, which typically holds the processed substrate (e.g., a semiconductor wafer). In this work, we demonstrate for the first time the existence of normal modes in electric potential analogous to the vibrational modes in circular membranes and plates. These modes are exhibited through cross spectral analysis of the plasma potential measured with an emissive probe at 208 spatial positions and sampled at 1 GHz. These modes exist at several frequencies and are described by a series of Bessel functions. The data further suggests a nonlinear interaction between modes of different frequencies.

Introduction.—In low temperature, nonequilibrium plasmas, ions are accelerated towards surfaces by highly directional electric fields resulting from potentials in the sheath and presheath regions. These fields and potentials have been studied and modeled by numerous researchers [1–9]. In recent years, a great deal of attention has been given to standing waves in capacitively driven plasmas [10–15]. Standing waves have been seen in high frequency capacitive discharges between closely spaced parallel plates. A model in slab geometry [16] was developed to predict the wavelengths of the modes. The model clearly indicates the presence of standing waves in a capacitive discharge for both symmetric and asymmetric devices. The wave pattern depends on both the gas pressure and driver frequency.

A capacitive applicator in this work is defined as an rf-driven electrode placed in contact with a glow discharge plasma generated by other means such as from an inductively coupled or microwave source. These applicators are typically used to accelerate ions towards a substrate in plasma processing applications. In this work, the radius of the applicator is 15 cm and it is isolated from ground by an approximately 4 cm aluminum oxide ring with an embedded electrode assembly. The normal modes observed in this experiment are analogous to the vibrational modes in circular membranes and plates. As the plasma is nonmagnetized, the modes can be determined using the two-dimensional scalar wave equation using the same solution techniques employed for vibrating membranes and plates. Mathematically, they are described as a linear combination of Bessel functions and a harmonic solution of sines and cosines in radial and angular coordinates, respectively.

An emissive probe [17,18], used to measure the plasma potential, V_p, is located 0.95 cm above the applicator and moved by a two-dimensional drive system. The heater current to the probe is switched off during the 100 μs

measurement to eliminate uncertainties due to the heater voltage. V_p is mapped at 208 spatial locations and digitized at 1 GHz. An electrically floating probe is located 1.84 cm above the center of applicator to afford a means to generate correlation functions for the detection of waves in the low temperature plasma. The experimental bulk plasma is produced by a low frequency (800 kHz) inductively coupled plasma (ICP) discharge. Two higher frequency (2 and 60 MHz) fields are applied simultaneously through the capacitive plasma applicator, and the vacuum chamber walls serve as the path for currents to return to ground. In other studies focused purely on capacitive discharges, the gap between electrodes (1–5 cm) is on the order of, or smaller than, twice the skin depth $\delta = \frac{c}{\omega_{pe}}$, where c is the speed of light and ω_{pe} is the electron plasma frequency. In this reactor, the gap height is approximately 17.5 cm or 7δ. An additional Langmuir probe is used to provide basic bulk plasma parameters ($n \cong 5 \times 10^{11}$ cm^3, $T_e \cong 3$ eV). A schematic of the plasma chamber and sheaths is shown in Fig. 1(a). The probe electronics for the pulsed emissive probe and drive systems are described elsewhere [18].
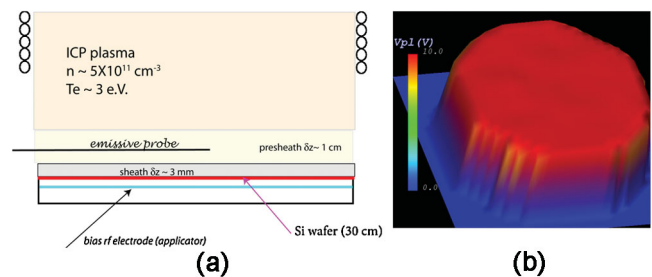

FIG. 1 (color). (a) Schematic of ICP coil, background plasma, and sheaths. The emissive probe is shown (the reference probe which is at a fixed position above it is not). The emissive probe which detects the wave is in the pre-sheath. (b) The 2D plasma potential measured by an emissive probe during the discharge. ICP source power is 450 W in argon at 5 mT.

The plasma potential, with no bias on the applicator, is shown in Fig. 1(b) for a 450 Watt ICP argon plasma at 5 mT; the plasma potential is constant over the entire capacitive applicator as expected. The measurements are 10 shot averages at each spatial position. The plasma potential does not drop to zero at the edge of the 30 cm (outer diameter) plasma applicator; rather, this is where the data acquisition plane is terminated. The electron temperature was also measured, and it is highly uniform and about 3 eV over the entire surface of the applicator.

When the dual frequency capacitive plasma applicator (at 2 and 60 MHz) and the inductive coupler are simulta- neously applied, it is postulated that standing waves can occur [10–12]. To better understand this phenomenon, correlation measurements are taken between the movable emissive probe and the stationary floating probe. To iden- tify any modes which may exist above the applicator plane, one cannot take a temporal average at each probe location and use it to build a two dimensional picture of the struc- ture; any random oscillatory events would be averaged out. Also, it is infeasible to put hundreds of macroscopic probes in the plasma as they would greatly perturb the system.

The correlation Cross Spectral Function (CSF) [19] is given by the following expression:

$$C(\vec{r}, \tau, \omega_0) = \frac{1}{N} \sum_{\text{shots}=1}^{N} \frac{\sum_t \{V_{\text{plas}}(\vec{r}, t + \tau, \omega_0) - \langle V_{\text{plas}}(\vec{r}, \omega_0)\rangle\}\{V_{\text{float}}(\vec{r}, t, \omega_0) - \langle V_{\text{float}}(\vec{r}, \omega_0)\rangle\}}{\sqrt{\sum_t [V_{\text{plas}}(\vec{r}, t, \omega_0) - \langle V_{\text{plas}}(\vec{r}, \omega_0)\rangle]^2 \sum_t [V_{\text{float}}(\vec{r}, t, \omega_0) - \langle V_{\text{float}}(\vec{r}, \omega_0)\rangle]^2}}. \tag{1}$$

V_{float} and V_{plas} are the two probe signals. First, they are filtered at frequency ω_0 using a digital filter. The average of the time series $\langle \rangle$ is subtracted from the series so that only the oscillating part remains. $\vec{r}$ is the vector separation of the probes (in this data set, there are 208 r values), and τ is the lag time. Suppose the signal is a propagating pulse. At some time t, the pulse has gotten to one probe but not the other, so when the signals are multiplied, you get nothing. At a given lag time, the signal could arrive at the second probe, so when you multiply them, you get a nonzero value. The denominator is the autocorrelation function, which normalizes C to ± 1. We then average this over a 15-shot ensemble (15 shots were chosen so each data run would take 4 hours).

The CSF data were all acquired with a fill pressure of 5 mT Ar. The reference probe, which is a small (3 mm diameter) Langmuir probe, is terminated by a 1 MΩ resis- tor. If the data are not filtered, the contribution from all harmonics gives a complex pattern as shown in Fig. 2. As time goes by, the pattern changes polarity and smaller features come and go. The pattern is the superposition of modes existing at the driver frequencies, and possibly their harmonics.

To explore this, the data were filtered and CSFs calcu- lated at individual frequencies. The CSF $C(f = 2.18$ MHz, x, y, $\tau)$ and a color bar indicating its value are shown at three delay times over the entire wafer in Fig. 3 Left. The first at a lag of $\tau_0 = 0$ μs, the second with a lag $\tau_1 = \tau_0 + 0.115$ μs, and the third $\tau_2 = \tau_0 + 0.230$ μs. The wave period is 0.459 μs. The pattern oscil- lates as an $m = 0$, J_0 (kr) standing mode much as the lowest order vibration of a drum. The CSF at 60 MHz, as a function of delay time at the center of the wafer, is shown in Fig. 3 Right. The 60 MHz wave has a 16.7 ns period; the 1 GHz digitization rate is adequate to track the signal. Figure 3 Right shows the spatial distribution of the CSF above the wafer at three values of the delay time τ. Unlike the CSF in the 2 MHz case, there is considerable structure

visible. The CSF does not appear to be azimuthally sym- metric as one would expect. The pattern suggests a dis- torted $m = 1$ mode. The pattern could be altered by changing the location of the reference probe whose shaft was always over the wafer. To test for this, a second CSF data run was acquired with the reference probe 3 cm from the edge of the wafer. The pattern was essentially the same in that case.

The data suggest that the CSF can be decomposed into a Fourier-Bessel series using only several terms. If F is the fit to the experimental data, and R the radius of the wafer:
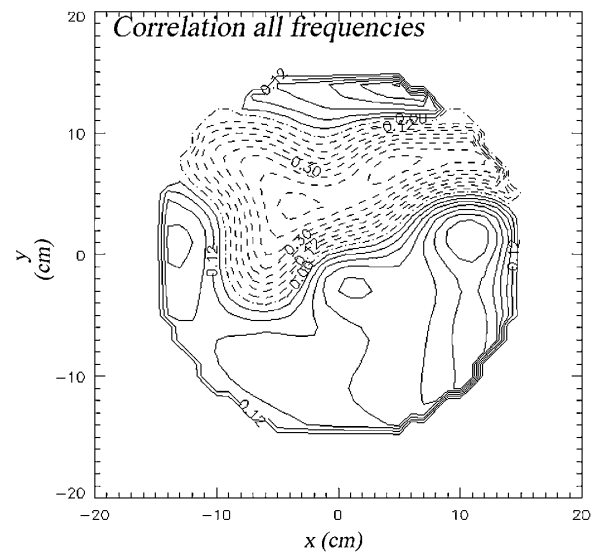

FIG. 2. Correlation function C (x, y, τ) between the emissive and floating probe 1.84 cm above the wafer (at $x, y = 0$) and at a lag time of 249 ns. All frequencies are included. At this time, the lowest value of C is -0.3 and the highest value is 0.15. The center of the wafer is at $x = y = 0$. The probe shaft for the movable motorized probe enters from $x = 20$, $y = 0$, Argon, 5 mT, 800 W (ICP), and 1 kW (2 MHz, 60 MHz). The correlation displays a complicated pattern, which changes in time.

$$F(r, \theta) = \sum_{n=0}^{N-1} \sum_{m=0}^{M-1} \left\{ a_{nm} J_n\left(\frac{z_{nm}r}{R}\right) \cos(n\theta) \right.$$
$$\left. + b_{nm} J_n\left(\frac{z_{nm}r}{R}\right) \sin(n\theta) \right\}. \quad (2)$$

This set of basis functions implicitly requires boundary conditions, i.e., the modes are set to zero at the edge of the wafer, $r = R$, for Dirichlet boundary conditions, exactly equivalent to clamped, vibrating membranes and plates. Data for the experiment is only available for the area above the wafer, not to the boundary at the chamber grounded surfaces (e.g., grounded walls and electrode assembly housing) where we could be sure this is a good assumption. However, investigation of analogous fits using Neumann or mixed Dirchlet and Neumann boundary conditions show that the broad character of the modes does not change appreciably. These latter boundary conditions are an analog to unclamped or partially clamped vibrating membranes and plates, respectively. In either case, the squared error term is $E^2 = \sum_{i=0}^{N-1} w_i [F(r_i, \theta_i) - f_i]^2$ where the sum is over all spatial locations with valid data, f_i. We perform a least squares fit by minimizing the error for each coefficient with the weighting function $w_i \equiv r_i$ to orthogonalize the series. For example, the first equation is $\frac{\partial E^2}{\partial a_{00}} = 2\sum_i w_i [F(r_i, \theta_i) - f_i] J_0(z_{00}r_i) = 0$ where we use a normalized radius with $0 \leq r_i \leq 1$ and z_{00} is first zero of J_0. The problem becomes one of matrix inversion for each coefficient. Figure 4 shows two fitting functions to the 60 MHz data shown in Fig. 3. In the left-hand panel, only $(m, n) = (0, 1)$. In the panel on the right, the indicies where Bessel functions up to $n = 4$ and m numbers of up to 4 were used in the fit. It is clear that when enough terms are used, the series approximates the data quite well as expected; however, the first two modes can be used as a rough approximation. A time series of the 60 MHz correlation shows that it is modulated by 5–10% at 2 MHz. This modulation may be reflected in the $m = 0$ component of the CSF. The CSF is normalized. A Fourier transform of the potential shows that the fluctuations at 60 MHz and its sidebands and harmonics are larger than those closer to 2 MHz. However, the 60 MHz CSF is clearly modulated by 2 MHz. The modulation is indicative of a nonlinear interaction, most likely in the plasma sheath, between the different harmonics.

Summary and conclusions.—For the first time, to these authors' knowledge, we have clearly observed normal modes of standing waves in the plasma potential at the fundamental frequencies of the bias voltages over the entire surface of a capacitive applicator. Higher harmonics are observed but are not analyzed here. A previous study [12] has provided evidence for the existence of standing waves through ion current measurements across the grounded electrode of a capacitively generated discharge. These measurements were time-averaged as the data acquisition was performed on time scales much larger than
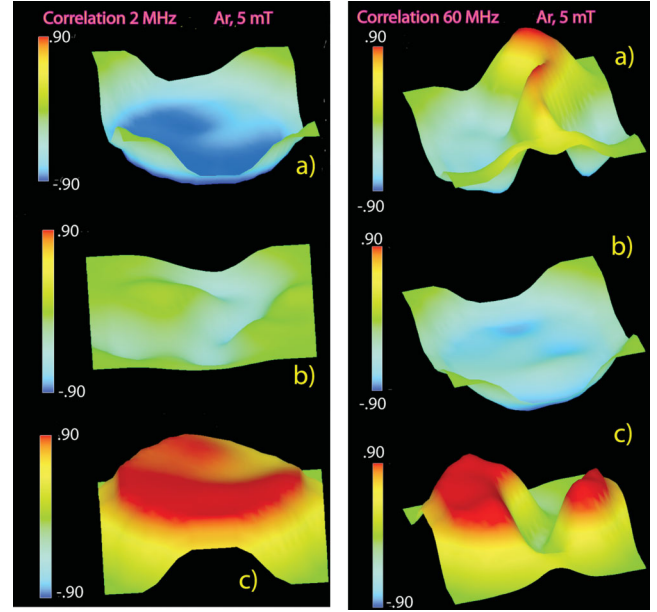

FIG. 3 (color). Left. Cross spectral function C ($f = 2.18$ MHz, x, y, τ). The three delays are (a) $\tau_0 = 0$ μs, (b) $\tau_1 = \tau_0 + 0.115$ μs (quarter period), and (c) $\tau_2 = \tau_0 + 0.230$ μs (half period) with respect to the first. Right. Cross spectral function filtered at 60 MHz over the wafer surface at three delay times each a quarter period apart. The three delays are (a) $\tau_0 = 0$ μs, (b) $\tau_1 = \tau_0 + 4.17$ ns (quarter period), and (c) $\tau_2 = \tau_0 + 8.33$ ns (half period) with respect to the first.

the rf periods, and, consequently, any ion current fluctuations whose average value is close to zero would not be observed. Furthermore, the normal modes in potential observed in this study would not affect the ion current density as the excitation frequency is well above the ion plasma frequency.

The observed normal modes in potential can be expressed as summations of Bessel functions much as the vibrational modes in circular membranes and plates. In the electrostatic limit, the Boltzmann relation links electron density to plasma potential fluctuations ($n = n_0 e^{(q\varphi/kT_e)}$). Consequently, these measurements suggest there will be fluctuations in the electron density above a processed sub-
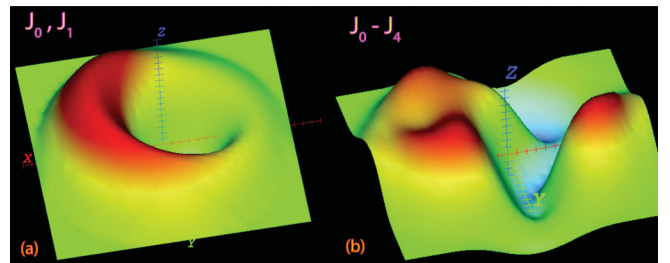

FIG. 4 (color). Bessel function fits to the 60 MHz data shown in Fig. 3(b). (a) $J_0(r)$ and $J_1(r)[^{\sin m\theta}_{\cos m\theta}]_{m=0,1}$. (b) Fit to the data for $(m, n) = (0 - 4, 0 - 4)$. This is to be compared to Fig. 3(b). The moving probe enters the system along the x axis from the right.

strate resting on a capacitive applicator that could affect local electron-neutral kinetic reactions. The modes are most likely excited by the oscillations of the plasma-sheath interface [1,2] including harmonic oscillations arising from the nonlinear mechanisms governing the sheath dynamics. As the frequency is increased, the order of the normal modes is postulated to increase as these modes are likely determined by the impedance terminating conditions on the chamber surfaces. Stray impedances (e.g., small reactive impedances) due to structural vacuum chamber subtleties such as substrate feedthroughs, pump and gas inlet ports, and isolation valves, for example, have a greater effect as the frequency is increased. These stray impedances are further hypothesized to affect the distribution of rf currents returning to grounded surfaces thereby influencing the magnitudes and directions of the current density vectors in the sheaths, presheaths, and bulk plasma. In the bulk, the rf currents are predominantly carried by electrons, and it is likely that the modes observed in this work have corresponding fluctuations in the density (and perhaps even the localized heating) of the electrons. Better understandings of these effects will undoubtedly improve uniform power coupling in plasma processing systems. Capacitive applicators of various kinds have been used in glow discharge processing plasmas for over 30 years; the physics is now catching up with the applications. Detailed study of waves, sheaths, and particle motion in these tools is ever more important to improving their performance and guiding in their future design.

[1] M. A. Lieberman, IEEE Trans. Plasma Sci. **16**, 638 (1988).
[2] V. A. Godyak and N. Sternberg, Phys. Rev. A **42**, 2299 (1990).
[3] M. S. Barnes, J. C. Forster, and J. H. Keller, IEEE Trans. Plasma Sci. **19**, 240 (1991).
[4] T. E. Nitschke and D. B. Graves, IEEE Trans. Plasma Sci. **23**, 717 (1995).
[5] M. E. Riley, Sandia Report No. 950775, 1995.
[6] N. Sternberg and V. A. Godyak, IEEE Trans. Plasma Sci. **31**, 665 (2003).
[7] J. Robiche, P. C. Boyle, M. M. Turner, and R. A. Ellingboe, J. Phys. D **36**, 1810 (2003).
[8] T. Mussenbrook, R. P. Brinkman, M. A. Lieberman, A. J. Lichtenberg, and E. Kawamura, Phys. Rev. Lett. **101**, 085004 (2008).
[9] P. A. Miller, E. V. Barnat, G. A. Hebner, A. M. Patterson, and J. P. Holland, Plasma Sources Sci. Technol. **15**, 889 (2006).
[10] J. E. Stevens, M. J. Sowa, and J. L. Cecchi, J. Vac. Sci. Technol. A **14**, 139 (1996).
[11] P. Chabert, J. L. Raimbault, P. Levif, and J. M. Rax, Phys. Rev. Lett. **95**, 205001 (2005).
[12] A. Perret, P. Chabert, J. P. Booth, J. Jolly, J. Guillon, and Ph. Auvray, Appl. Phys. Lett. **83**, 243 (2003).
[13] H. Schmidt, L. Sansonnens, A. A. Howling, Ch. Hollenstein, M. Elyaakoubi, and J. P. M. Schmidt, J. Appl. Phys. **95**, 4559 (2004).
[14] P. Chabert, J. L. Raimbault, J. M. Rax, and M. A. Liberman, Phys. Plasmas **11**, 1775 (2004).
[15] P. Chabert, J. Phys. D **40**, R63 (2007).
[16] I. Lee, D. B. Graves, and M. A. Liberman, Plasma Sources Sci. Technol. **17**, 015018 (2008).
[17] D. Lee, Y. H. Ting, L. Oksuz, and N. Hershkowitz, Plasma Sources Sci. Technol. **15**, 873 (2006).
[18] P. Pribyl, W. Gekelman, S. Vincena, K. Kuns, and M. S. Barnes, Rev. Sci. Instrum. (to be published).
[19] J. S. Bendat and A. G. Piersol, *Random Data* (Wiley Interscience Press, New York, 2000), 3rd ed.